Received: Added at production | Revised: Added at production | Accepted: Added at production
DOI: xxx/xxxx

RESEARCH ARTICLE

Efficient Land Desertification Detection using a Deep Learning-Driven Generative Adversarial Network Approach: A case study

Nabil Zerrouki[1] | Abdelkader Dairi [2,3] | Fouzi Harrou*[4] | Yacine Zerrouki[5] | Ying Sun[4]

[1]DI2M team, Center for Development of Advanced Technologies, Baba Hassen 16081, Algiers, Algeria

[2]University of Sciences and Technology Houari Boumédienne, LCPTS, Faculty of Electronics and Computer Science, Algiers, Algeria

[3]Department of Computer Science, University of Science and Technology of Oran-Mohamed Boudiaf (USTO-MB), Bir ElDjir 31000, Algeria

[4]King Abdullah University of Science and Technology (KAUST), Computer, Electrical and Mathematical Sciences and Engineering (CEMSE) Division, Thuwal, 23955-6900, Saudi Arabia.

[5]Conservatoire National des Formations à l'Environnement, Bab El Oued 16000, Algiers, Algeria

Correspondence
*Fouzi Harrou, King Abdullah University of Science and Technology, Thuwal, 23955-6900, Saudi Arabia.
Email: fouzi.harrou@kaust.edu.sa

Funding Information
This work was supported by funding from King Abdullah University of Science and Technology (KAUST), Office of Sponsored Research (OSR) under Award No: OSR-2019-CRG7-3800.

Abstract

Precisely detecting land cover changes aids in improving the analysis of the dynamics of the landscape and plays an essential role in mitigating the effects of desertification. Mainly, sensing desertification is challenging due to the high correlation between desertification and like-desertification events (e.g., deforestation). An efficient and flexible deep learning approach is introduced to address desertification detection through Landsat imagery. Essentially, a Generative Adversarial Network (GAN)-based desertification detector is designed and for uncovering the pixels influenced by land cover changes. In this study, the adopted features have been derived from multi-temporal images and incorporate multispectral information without considering image segmentation pre-processing. Furthermore, to address desertification detection challenges, the GAN-based detector is constructed based on desertification-free features and then employed to identify atypical events associated with desertification changes. The GAN-detection algorithm flexibly learns relevant information from linear and nonlinear processes without prior assumption on data distribution and significantly enhances the detection's accuracy. The GAN-based desertification detector's performance has been assessed via multi-temporal Landsat optical images from the arid area nearby Biskra in Algeria. This region is selected in this work because desertification phenomena heavily impact it. Compared to some state-of-the-art methods, including Deep Boltzmann Machine (DBM), Deep Belief Network (DBN), Convolutional Neural Network (CNN), as well as two ensemble models, namely Random Forests and AdaBoost, the proposed GAN-based detector offers superior discrimination performance of deserted regions. Results show the promising potential of the proposed GAN-based method for the analysis and detection of desertification changes. Results also revealed that the GAN-driven desertification detection approach outperforms the state-of-the-art methods.

KEYWORDS

Received: Added at production | Revised: Added at production | Accepted: Added at production
DOI: xxx/xxxx

Deep learning, generative adversarial networks (GAN), desertification detection, Landsat data, land cover changes.

1 | INTRODUCTION

Accurate estimation of land cover changes is crucial for the retrieval of several land cover degradations. The availability of remote sensing data repositories, practically with revisit periods of Earth observation satellites offering multi-date imagery, has received an important consideration in the land cover monitoring research field [1, 2]. Over the last few years, various applications like evaluating burned areas, observation of pollution evolution, the assessment of deforestation, and desertification detection have been proposed in the literature [3-7]. In the present paper, we focus on the desertification phenomenon, which is generally known as one of the most vital problems of Land Cover Change Detection (LCCD), mainly because of its undesirable impacts on water resources, agriculture areas, and soil moisture. Given the Saharan areas' size, time-series imagery remains the keyway for observing sand movement and detecting regions affected by desertification phenomena. Various studies and research projects have been launched to design reliable desertification detection models to prevent the environment and improve the daily life quality of the local population [3, 5]. For instance, in [1], an approach using spectral mixture analysis (SMA) and a decision-tree algorithm has been proposed for analyzing the grassland desertification in Ningxia, China using Landsat time-series images. In [9], a method based on fuzzy spatiotemporal data with UML modeling language is applied for desertification detection over a time interval of 40 years (1970– 2010). The data is viewed as a timeline, where historical and topological states were incorporated in the model to make it dynamic considering the development process of the desertification data. The region of Alashan, China, has been chosen as a study region for analysing the dynamics of different desertification types in the past 40 years. In [10], to assess the degree of sand movement effect, a desertification difference index (DDI) has been derived from the negative correlation between albedo and Normalized Difference Vegetation Index (NDVI). They assume that the desertification phenomenon is an uncertain process and employ an analysis approach in desertification assessment. Several time-series data from MODIS sensors were selected, corresponding to the regions of interest in central North America, eastern Asia, the Pacific Rim, and central Australia between 2000 and 2014.

In [11], a similarity metric has been invoked to estimate desertification using Topsoil Grain Size Index (TGSI), NDVI, and land surface albedo. A decision tree (DT) approach is then employed to evaluate the evolution of desertification in the protected zone named the Hogno Khaan during the periodes1990, 2002, and 2011. To measure the degree of vegetation degradation caused by desertification effects at western Rajasthan, India, in [12], a correlation analysis between residual trend and rain-use efficiency (RUE) and NDVI was presented during the period between 1983 and 2013. The authors in [13] utilized Landsat images satellite time series over 30 years (1984–2013) based on the Tasselled Cap transform. Particularly, an ensemble of parameters for the Tasselled Cap transform have been added to enhance understanding of dryland conditions in the city of Azraq Oasis, Jordan. Recently, authors in [14] designed a deep learning strategy using a convolution neural network (CNN) to uncover oasis desert by on-board sensors of Unmanned Aerial Vehicles (UAV) and remote sensing imagery. This work aims to design an approach for estimating plant communities' degradation in oasis-desert for desertification prevention in the Taklamakan Desert, northwestern China. Results show that the achieved correct detection rates when using VGG16 and VGG19 are 93.8 % and 96.73%, respectively.

In [15], in addition to NDVI, several sensitive parameters for desertification assessment were investigated, including TGSI, modified soil adjusted vegetation index (MSAVI), and land surface albedo. An approach based on thresholding has been applied to discriminate distinct

Received: Added at production | Revised: Added at production | Accepted: Added at production
DOI: xxx/xxxx

levels of desertification in regions of Naiman Banner, China. It has been shown that the non-linear Albedo-MSAVI feature space modelling obtained the best output corresponding to an overall accuracy of 90.1%. In [33], the authors proposed a new desertification detection index using thermal infrared emissivity data. Compared to the NDVI parameter, Sand Differential Emissivity Index (SDEI) distinguished between very close classes and presented a high degree of similarities like desertified land and dry vegetation region. A threshold-based formalism was applied as a classification method, where several simulations were conducted using ASTER Global Emissivity Dataset covering the region of Gurbantonggut Desert, Xinjiang, China. In [34], an analysis of the spatiotemporal evolution of dune migration is conducted. Both least-squares adjustment and singular values decomposition techniques were exploited to investigate dune movement using optical imagery acquired by Landsat 8 and Sentinel 2 satellites from 2013 to 2018. In [15], the authors address the problem of separability between pixels presenting desertified regions and the rest of land cover types, where several existing feature space models, namely land surface temperature (LST), MSAVI, NDVI, TGSI, and Albedo, have been combined to construct multiple feature spaces. Landsat and OLI (operational land imager) images with a spatial resolution of 30 m were utilized. These images were acquired between 1989 and 2017, covering Naiman Banner and Tongliao City, Mongolia. The overall classification rates of the proposed feature spaces are comprised between 86.54 % and 95.51%. Note that the desertification issue is often raised in Algeria, where numerous arid regions suffer from the desertification effects. As a result, several research studies have been proposed to tackle this issue to map and identify the spatial and temporal movement of desertification using Remote Sensing data. In [16], the authors analyzed land degradation and desertification dynamics in two areas in North Africa, namely Oum Zessar (Tunisia) and Biskra (Algeria), based on remote sensing imagery. To this end, they proposed a combined approach merging the desirable features of the decision tree (DT) with the Isodata algorithm and then apply it to the principal components obtained from Knepper ratios. Results show that the reached correct detection rate is 79.97%. In [17], a pixel-based technique using the Maximum Likelihood method has been introduced to detect desertification due to the mobile dune phenomenon in southern Algerian Sahara. In [8], to evaluate the land cover degradation in Biskra (Algeria) based on optical Landsat image series, the support vector machine is applied for object classification on the change indices as features. The result shows that overall accuracy of 95.15% was reached.In recent years, with the advancement of deep learning models, several methods have been introduced to improve time-series modeling and anomaly detection in various domain applications [22-24]. Basically, deep learning models can be obtained by concatenating several layers into the neural network structures [25]. The main feature of deep learning models is their ability to automatically extract pertinent information from large data. Also, they proved to be useful in dealing with different types of datasets, including time-series [29, 30], videos [31], images, and audio datasets [32].

During recent years, Generative Adversarial Networks (GANs) have shown good efficacy to synthesize visually appealing images [25]. A GAN essentially comprises two networks: the generator network G and the discriminator network D [25]. The generator attempts to learn the distribution underlying the input data and then generate new data points following the learned distribution to elude the discriminator, which aims distinguishing real data points from fake ones [26]. GANs give a promising strategy to avoid the overfitting phenomena [35]. Thereby, the GANs desirable features have been exploited in numerous applications, including text-to-image synthesis [26], face synthesis [27], and single image super-resolution [28]. Essentially,

Received: Added at production | Revised: Added at production | Accepted: Added at production
DOI: xxx/xxxx

this study investigates the effectiveness of the GAN-based approach in addressing the desertification detection issue, where the input data are time-series data instead of images.

In this paper, using the generative adversarial network (GAN)-based scheme for desertification detection is investigated for the first time. To this end, as an input, it uses multitemporal Landsat optical images from the arid region around Biskra in Algeria. To the best of the authors' knowledge, a combination of Landsat images and a GAN-driven deep learning approach has not yet been investigated in identifying desertification propagation. Note that the major advantage of using generative models for classification problems is that they can first be trained in an unsupervised way and later fine-tuned to deal with the classification task based on the softmax layer. Crucially, GANs are a generative composite model based on two players zero-sum approach, where it consists of two parts generator and discriminator trained to learn the training data distribution, which is different from the Markov chain Monte Carlo (MCMC) that used Gibbes sampling to train RBM-based models, such as DBN and DBM. GAN architecture is flexible, enabling to choose any neural network architecture as generator or discriminator resulting in a deeper model able to learn more complex features and map them efficiently to their target classes. It has been shown that the GAN-based desertification detector achieves better performance in terms of classification accuracy, and the overfitting problem can be considerably mitigated. The GAN-based desertification detector's performance has been assessed via multi-temporal Landsat optical images from the arid area nearby Biskra in Algeria. This region is selected in this work because desertification phenomena heavily impact it. Compared to three commonly used deep learning methods, namely Deep Boltzmann Machine (DBM), Deep Belief Network (DBN), Convolutional Neural Network (CNN), as well as to two ensemble models, namely Random Forests and AdaBoost, the proposed GAN-based detector offers superior discrimination performance of deserted regions. Results show the promising potential of the proposed GAN-based method for the analysis and detection of desertification changes. Results also revealed that the GAN-driven desertification detection approach outperforms the state-of-the-art methods.

In the next section, we elucidate the proposed GAN-based desertification detector in detail. The third section offers the involved multi-temporal satellite datasets and discusses the discrimination results and comparisons. Lastly, in the fourth section, we conclude this study.

2 | PROPOSED DESERTIFICATION FRAMEWORK

Figure 1 illustrates an overview of the proposed detection framework. Figure 1 shows that the proposed method includes four principal steps: image acquisition, pre-treatment, feature extraction, and desertification detection. In this section, the background elements of the proposed approach are provided.

Received: Added at production | Revised: Added at production | Accepted: Added at production
DOI: xxx/xxxx

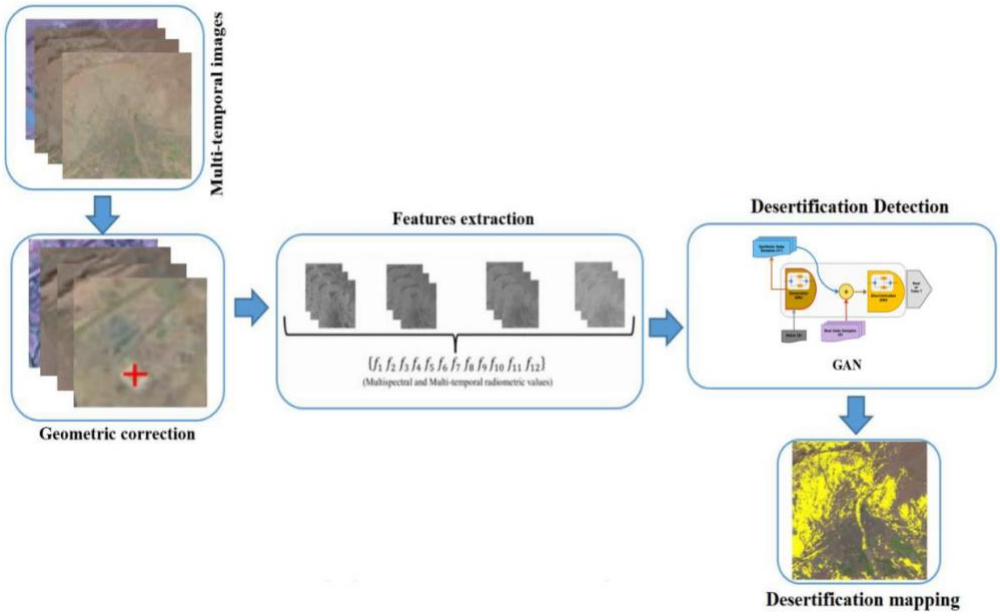

Figure 1 Framework of the designed desertification detector.

2.1 | IMAGE PRE-PROCESSING AND CHARACTERISTIC GENERATION

It is noteworthy that in optical imagery (aerial or remote sensed data), radiometric values vary according to numerous parameters, such as land surface slope and its angle of orientation, the atmospheric factors, and practically on the nature of the observed land surface, which usually represents the goal of the exploration [18, 19]. In many cases, the pre-processing step is essential and generally includes several adjustments, such as atmospheric normalization, radiometric calibration, and geometric correction. Here, we used ground control points to achieve the radiometric correction. The main particularity of these control points is their invariance in the multi-temporal images. In this case, with multi-temporal and multi-spectral images, 120 control points have been located for the co-registration phase. Note that the control points are selected mainly by using a visual examination and our knowledge about the investigated region.

Feature extraction or generation is a critical step in the recognition process since the designated attributes powerfully influence the recognition results. The generated attributes should be descriptive enough to achieve a suitable recognition rate and not too complex to enable reasonable processing time. Conventionally, extracting features (radiometric, spectral, or textural) is performed using some renowned remote sensing softwares, such as ENVI or eCongnition [8, 18]. However, softwares do not allow an adequate manipulation of the data since certain processing details remain unknown, and in many cases, they are considered black boxes.

The variation of pixel's radiometric values (generally assimilated to spectral signatures in different wavelengths) is an efficient aspect of evolution in thematic scenes. This variation can be utilized as a significant factor in identifying thematic classes and detecting regions suffering from sand movement over time through multi-temporal images. The significant aspect of spectral signatures can be decisive in the decision phase. For example, abrupt land cover evolutions, such as natural catastrophes or disasters, radiometric responses will experience a high degree of change (sudden increase or decrease), while land cover evolutions, such as growing urban, generate a comparatively smooth dissimilarity in spectral radiometric responses. Furthermore, pixels presenting some false LCCs produced (i) by seasonal climate effects such as aridness areas or (ii) by human effects like degradation and lessening forest areas are frequently classified as desertified pixels. This misclassification is due to the strong

Received: Added at production | Revised: Added at production | Accepted: Added at production
DOI: xxx/xxxx

resemblance between the evolution mode of their respective characteristics through time (desertification and like-desertification cases). In the present study, an observation sequence that describes radiometric reflectance in diverse spectral bands (3 channels) is associated with every multi-temporal response (T_1, T_2, T_3 and T_4). Since remote sensing scenes are adapted to a sequential observation, characteristics extracted using different scenes have been concatenated to obtain one entire feature vector.This amounts to meaning that each pixel is represented by twelve attributes (f_1 ... f_{12}), which can be assimilated to the multi-temporal and multi-spectral signatures, as illustrated in Figure 2.

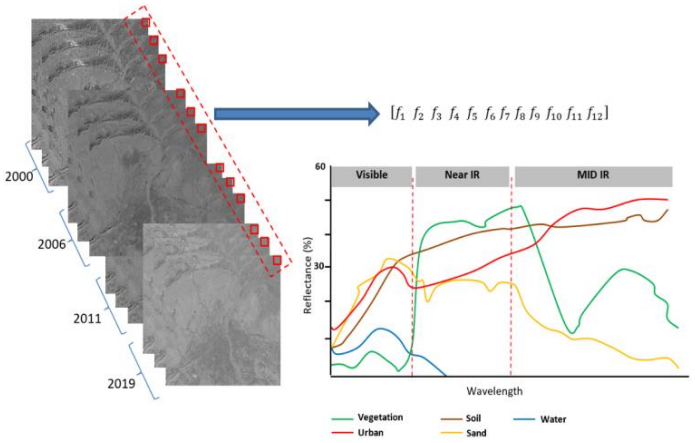

Figure 2 The extracted multi-temporal and multi-spectral features.

This concatenation answers the needs of feature representation and extends some traditional data organization variants by freely acting on each pixel separately (by disclosing their textural links or local structures, unlike the object approach, which needs the segmentation phase). The main advantage of this feature representation is constructing latent structures within the radiometric data by exploring multi-spectral and multi-temporal information associated with each pixel's feature vector.

Furthermore, the use of a reduced number of attributes through a feature vector with a relatively small size (12 multi-temporal and multi-spectral features in our case), unlike hyper-spectral values or transformed attributes as characteristics, permits the manipulation of pertinent features with a minimal degree of correlation between features. It is worth noting that the use of entirely uncorrelated or independent characteristics remains difficult to ensure for real-world classification tasks. In our case, no prior feature selection or dimensionality reduction phase (to remove unnecessary and redundant information) is required. Generally speaking, classification algorithms perform better using input features with simpler inter-dependencies.

2.2 | GENERATIVE ADVERSARIAL NETWORKS (GANS)

GANs are efficient deep learning models able to learn complex data representations and capture data distributions without any need for labeling (i.e., in an unsupervised manner) [35, 36]. GANs are similar to RBM and VAE that belong to generative models, also known as probabilistic, where the main objective is to model high-dimensional distributions of data through the probability distribution approximation. However, GANs are a distinct and promising strategy, working in a collaborative way represented by a composite architecture. Specifically, they are composed of two neural networks arranged in an adversarial way in competition with each other named respectively: generator $\mathcal{G}$ and discriminator $\mathcal{D}$. The generator's role is to generate synthetic data (called fake data), which are incredibly comparable to the real input data, by introducing noise. The discriminator uses the generated data and the real data for the training phase (Figure 3). Real data is the measurements gathered from the

Received: Added at production | Revised: Added at production | Accepted: Added at production
DOI: xxx/xxxx

studied system or process. At this stage, the discriminator is trained using both fake and real data as input. Hence, the discriminator aims to separate real data and fake data. The optimal results are essentially obtained by using the competition of two deep learning networks such that $\mathcal{D}$ achieves superior discriminative capacity, and $\mathcal{G}$ suitability mimics the fake data that have approximatively identical distribution to the real data. Note that the generated data from a GAN model could be utilized as training data. Accordingly, the overfitting problem in deep models can be bypassed when only small-sized training data is available.

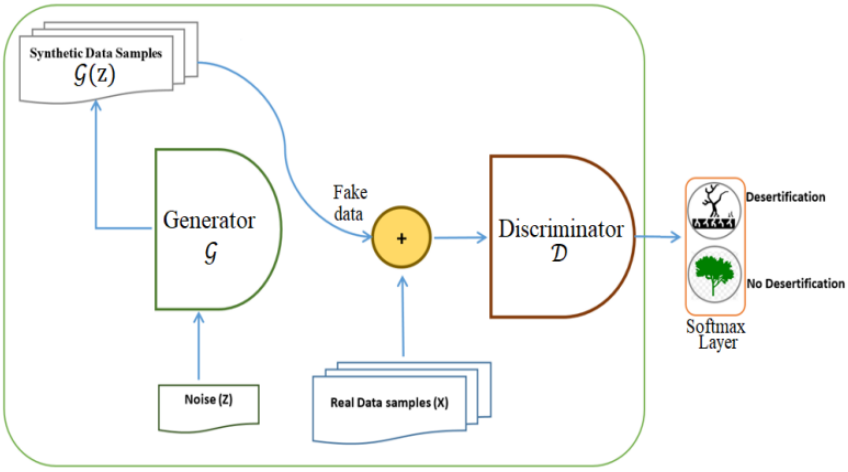

Figure 3 GAN-driven desertification detection framework.

Let us denote P$\mathcal{G}$(z) a prior distribution on input noise, $\mathcal{P}_{data(x)}$ the real data probability distribution and $\mathcal{P}_{g(x)}$ the distribution of samples generated by the generator. Indeed, measurement noise z is introduced in the generator $\mathcal{G}$ and fake data $\mathcal{G}$(z) are generated, which will be inputted into the discriminator $\mathcal{D}$. Subsequently, the generated data $\mathcal{G}$(z) or real measurements x are introduced into the discriminator $\mathcal{D}$, and the $\mathcal{D}$ will decide between $\mathcal{G}$(z) and x by computing the likelihood $\mathcal{D}(\mathcal{G}(z))$ and $\mathcal{D}(x)$ that $\mathcal{G}$(z) and x belongs to the data x or $\mathcal{G}$(z). In the training stage, the discriminator $\mathcal{D}$ parameters,θ, are adjusted for maximizing $log\mathcal{D}(x)$, which denotes the probability to determine the true origin of the input. Also, the generator G parameters, ϕ, are adjusted for minimizing $log(1-\mathcal{D}(\mathcal{G}(z)))$, which indicates the capacity of $\mathcal{G}$ to generate fake measurements as close to real as possible. In summary, the GAN training aims to solve the following minimax problem based on training datasets.

$$min_G max_D v(\mathcal{G},\mathcal{D}) = \mathbb{E}\,\mathcal{P}_{data(x)}[log\mathcal{D}(x)] + \mathbb{E}\,\mathcal{P}_{g(x)}[lo\,g(1-\mathcal{D}(\mathcal{G}(z)))], \quad (1)$$

where V($\mathcal{G}$, $\mathcal{D}$) denotes the GAN cost function and $\mathbb{E}$ refers to the mathematical expectation value. The stochastic gradient used by the discriminator to update its parameters during the training process is expressed as:

$$\nabla\theta_d \frac{1}{m}\sum_{i=1}^{m}[\,log\mathcal{D}\left(x^{(i)}\right) + log(1-\mathcal{D}\left(\mathcal{G}(z^{(i)})\right))\,] \quad (2)$$

Hence, the generator updates the model parameters based on a descending stochastic gradient computed as:

$$\nabla\theta_g \frac{1}{m}\sum_{i=1}^{m}[lo\,g\left(1-\mathcal{D}\left(\mathcal{G}(z^{(i)})\right)\right)] \quad (3)$$

After several iterations in training, the discriminator $\mathcal{D}$ can converge as:

$$\mathcal{D}^*(x) = \frac{P\,data(x)}{Pdata(x)+Pg(z)}, \quad (4)$$

where the training data distribution is denoted by Pdata(x), while Pg(z) represents the learned distribution. The main objective of the GAN training is to encourage the generator to produce a distribution P g(x) closest to the real data P data(x).

Received: Added at production | Revised: Added at production | Accepted: Added at production
DOI: xxx/xxxx

2.3 | MODEL TRAINING

This section provides more details about the proposed approach's learning process and the used models: DBN, DBM, and CNN. The GAN training process aims to learn approximating the training dataset probability distribution by encouraging the generator to produce samples closest to those of the training dataset and train the discriminator to distinguish actual data from the fake one. In other words, the discriminator $\mathcal{D}$ is trained to maximize the assigned probability to the real data, while the $\log(1-\mathcal{D}(\mathcal{G}(z))$ is minimized (usually called a two-player minimax game). The GAN training procedure can be summarized briefly (see Algorithm 1): updates the discriminative distribution to separate the samples from the data-generating distribution $\mathcal{P}_{data(x)}$ and those of the generative $\mathcal{P}_{g(x)}$.

Note that the desertification detection problem consists of classifying data input in typical observations (i.e., no deserted area) and abnormal observations (i.e., deserted area). To this end, an output layer is embedded into the GAN model to attribute an appurtenance probability for each class using a classifier with a Softmax activation function. Moreover, the entire model GAN+Softmax is trained in a supervised learning way for classification purposes; this step is called fine-tuning, aiming to adjust the model parameters.

In this study, the proposed approach's performance is compared to two powerful unsupervised generative models, namely DBN and DBM. The learning approach used in DBN and DBM is based on Markov chain Monte Carlo (MCMC) using Gibbs sampling to approximate the training dataset's data probability distribution, which is the first step of the training procedure. A softmax layer is also incorporated to DBN and DBM models as an output layer to learn how to classify the given input by providing a probability for each class. Here, a fine-tuning is conducted for optimizing the model parameters to address the discrimination problem. Furthermore, we compared the GAN-driven model to a convolutional neural networks (CNN) model, a supervised model. The CNN training aims to learn directly to classify the input; first a feature extraction step is done through multiple convolutions, and max-pooling operation, fully connected layers and a softmax layer compose the CNN model.

The final step in the recognition process consists of extracted features to the softmax layer, which converts the encoded vectors into conditional probabilities belonging to one of the two classes. In fact, in the case of two classes problem (undeserted and desert regions), one can utilize (i) softmax with two outputs or (ii) just one binary output. In the present case, a sigmoid (logistic) function is employed to model the conditional probability of the output, as follow:

$$p(w_i|x,\theta) = \frac{\exp(\theta_l^T x)}{\sum_k \exp(\theta_k^T x)}, \tag{5}$$

where $p(w_i|x,\theta)$ denotes the predicted conditional probability of the samples x belonging to the class j, while θ represents the model parameters.

It is worth remembering that in the case of binary classification, the probabilities sum is equal to one presenting one degree of freedom. Basing on this degree of freedom, one can formulate the conditional probabilities (of both classes) as follows:

$$p(w_1|x,\theta) = \frac{1}{1+\exp(\theta^T x)}, \tag{6}$$

$$p(w_2|x,\theta) = 1 - \frac{1}{1+\exp(\theta^T x)} = \frac{\exp(\theta^T x)}{1+\exp(\theta^T x)}. \tag{7}$$

The classification layer computed cross-entropy loss in the learning process as a loss function for separating different classes. The cross-entropy cost function was widely used in solving classification problems due to its adaptation with data learning probabilistic models applied in various fields. Typical cross-entropy formula is given as:

$$E(\theta) = \sum_i \sum_j y_{ij} \log p(w_j|\theta, x), \tag{8}$$

Received: Added at production | Revised: Added at production | Accepted: Added at production
DOI: xxx/xxxx

where y_{ij} represents 1-hot encoding of the sample label i. In the case of binary classification, the variable y_{ij} takes the value of 1 (if the sample is assigned to class 1), or the value 0 (if it is assigned to class 2) instead of 1-hot encoding of the sample label i. The binary cross-entropy loss formula is then expressed as:

$$E(\theta) = \sum_{i} y_i \log p(w_1|x,\theta) + (1 - y_i)\log(1 - p(w_1|x,\theta)) \quad (9)$$

Finally, the model parameter θ is updated at every back-propagation step t, using the RMSProp technique [20]:

$$G_t = \gamma G_{t-1} + (1-\gamma)(\nabla_\theta L(\theta_t))^2, \quad (10)$$

$$\theta_{t+1} = \theta_t - \frac{\eta}{\sqrt{G_t+\epsilon}} \nabla_\theta L(\theta_t), \quad (11)$$

where the parameters γ, η and L denote the momentum, the learning rate, and the averaged loss function over a mini-batch, respectively.

Algorithm 1: Training of GAN procedure.

Algorithm 1: Training of Generative Adversarial nets

Input : Training dataset $X = \{x^1, \ldots, x^k\}$
Output: {θ, ϕ}
θ : Discriminator model parameters;
ϕ : Generator model parameters;
m: number of mini-batch (drawn from full dataset);
{θ, ϕ} ← Initialize model parameters randomly;
SGA: Stochastic Gradient Ascendant;
SGD: Stochastic Gradient Descendant;
for n : training iterations **Do**
  for s steps **Do**
    Generator: sample m mini-batch of noise samples;
    $Z_m \sim \mathcal{P}_g(z)$;
    Discriminator : sample m mini-batch of observation;
    $X_m \sim \mathcal{P}_{data}(x)$;
    $SGA_d = \nabla\theta\ [log\mathcal{D}(X_m) + log(1 - \mathcal{D}(\mathcal{G}(Z_m))]$;
    θ ← update model parameters (SGA_d, θ);
  end
  Generator : sample m minibatch of noise samples: $Z_m \sim \mathcal{P}_g(z)$;
  $SGD_d = \nabla\theta\ [log(1 - \mathcal{D}(\mathcal{G}(Z_m))]$;
  ϕ ← update model parameters (SGA_g, ϕ);
end

Received: Added at production | Revised: Added at production | Accepted: Added at production
DOI: xxx/xxxx

3 | RESULTS AND DISCUSSION

3.1 | DATA DESCRIPTION

This part is dedicated to assessing the introduced strategy's effectiveness in separating pixels affected by desertification from unchanged pixels. To this end, multi-temporal satellite images have been investigated from the accessible database of the United States Geological Survey (USGS). Such image scenes include the same study region of Biskra (Figure 4) but are acquired at diverse periods: 2000, 2006, 2011, and 2019.

Figure 4 The investigated region situated in Biskra city, Algeria.

In fact, several years between the collections of images are deliberately chosen to enable us to perceive the propagation of sand region and recognize various changes, like the appearance of new urban agglomerations, building operations, deforestation regions, and large reforestation operations.

The study area (around the city of Biskra) is presented in Figure 4. The choice of the region of Biskra was not arbitrary since the phenomenon of desertification seriously impacts this region. Notably, the wind direction impacts sand movement and the local topographic factor in the sloping terrain. Furthermore, the location of mountains in the north direction promotes sand accumulation in the area.

It should be noted that the satellite scenes are also deliberately selected with low cloud appearance to simplify monitoring of sand movement. Indeed, images containing clouds may distort the pixels' radiometric values and masks the significant information, which generates multiple false detections.

Note that the four satellite images used in this evaluation have been acquired with the same spatial resolution of 30 meters per pixel. The selected images' principal properties are listed in Table I. Figure 5 illustrates the three bands' composition (red, green, and blue bands) of the used remotely sensed images acquired at distinct time points. The chosen region in this work is an arid area in the Algerian northeastern (around the city of Biskra) and often renowned as the Door of the Desert.

Received: Added at production | Revised: Added at production | Accepted: Added at production
DOI: xxx/xxxx

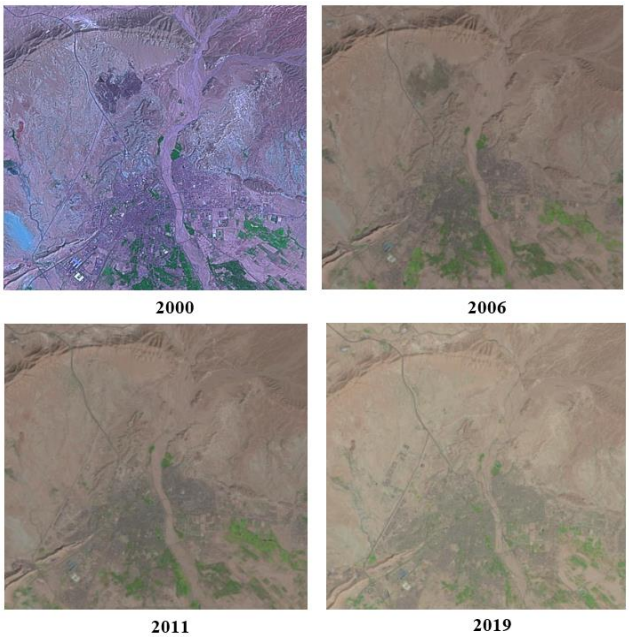

Figure 5 Three bands illustration of the four satellite images taken at distinct periods.

Table 1 The Selected Images' Main Properties.

Acquisition Date	Landsat ID N	Path/ Row	Processing Software Version	Data type	Solar azimuth	Solar elevation
03/09/2019	LC 08	194/ 036	LPGS 13.1.0	OLI_TIRS L1TP	139.55	56.76
05/03/2011	LT 05	194/ 036	LPGS 12.8.2	TM_L1TP	143.02	42.13
19/02/2006	LT 05	194/ 036	LPGS 13.0.1	TM_L1TP	145.86	37.47
15/04/2000	LE 07	194/ 036	LPGS 12.8.3	TM_L1TP	133.81	57.49

3.2 | DESERTIFICATION DETECTION RESULTS AND DISCUSSION

For a more effective evaluation of the proposed techniques in desertification detection application, in this study, only a subarea of the overall scene was considered in the experiment. This subarea was selected for further analysis, which describes 400x400 pixels. The choice of this subarea was mainly based on our level of knowledge concerning the study region.

The GAN classification is evaluated and compared to several powerful deep learnoing algorithms (DBN, DBM, and CNN) and two ensemble models (i.e., RF and AdaBoost procedures). Each model's optimal parameters are carefully chosen (parameter tuning phase) using the training data based on the grid search procedure. Table II lists the deep learning models' parameters employed in this study. For the RF algorithm, we used ten trees in the forest, and Gini impurity “Gini” is used to measure the quality of a split, and the maximum depth of the

Received: Added at production | Revised: Added at production | Accepted: Added at production
DOI: xxx/xxxx

tree is chosen 2. For the AdaBoost classifier, we used the 'SAMME.R' algorithm and ten learners to construct the AdaBoost procedure, and the learning rate is chosen 1. Decision Tree is used as the base learner from which the AdaBoost classifier is built.

Table 2 The values of the parameters used in GAN, DBN, DBM, and CNN.

Model	Layers	Epochs	Optimize	learning rate	Loss
DBN	2	500	Rmsprop	0.0001	Binary cross-entropy
DBM	3	500	Rmsprop	0.0001	Binary cross-entropy
CNN	3	200	Rmsprop	0.0001	Binary cross-entropy
GAN	3	300	Rmsprop	0.0001	Binary cross-entropy

The constructed GAN model consists of two parts, a Discriminator, a deep neural network composed of three layers.

- The input layer is composed of 8 neurons,
- The first hidden layer contains 24 neurons with ReLU (Rectified Linear Unit) as an activation function, and
- The second Hidden Layeris composed of 8 neurons with the Sigmoid as an activation function.

The Generator is also a deep neural network composed of four layers.

- The input layer is composed of 12 neurons
- The first hidden layer is composed of 24 neurons with ReLU as an activation function.
- The second hidden layer is composed of 8 neurons with Tanh as an Activation function.
- The output layer is composed of 2 neurons with the Softmax as an activation function.

3.3 | MEASUREMENTS OF EFFECTIVENESS

We used several statistical metrics to assess the performance of the investigated methods, namely true positive rate (TPR), false-positive rate (FPR), overall accuracy (OA), precision, F1 score (F-measure), and area under curve (AUC) [21]. OA is the widely employed measurement, which is computed from diagonal components of the confusion matrix. It denotes the ratio between pixels appropriately recognized (considering both classes: undeserted and deserted samples) and the whole number of pixels. The average accuracy can also be defined as follows:

$$\mathrm{OA} = \frac{\mathrm{TPR+TNR}}{\mathrm{TPR+TNR+FPR+FNR}}, \tag{12}$$

where TNR, FNR denote respectively true negative and false negative rates.

The ROC curve is also the commonly conducted graphical effectiveness statistic. It characterizes differences among sensitivity related to the TPR and specificity associated with the FPR. For effectiveness assessment, the AUC is an efficient factor for evaluating classification performance. In general, an AUC of 1 characterizes a perfect separation, while the value of 0.5 for an AUC characterizes coincidental (by chance) recognition. We also assessed the classification performance via F-measure (also known as F1Score). This parameter highlights the effect of the random separation degree. F-measure is computed by the use of recall (r) and precision (p) parameters. The recall value denotes the rate of true-positive cases (tp) to the overall numbers of pixels in the positive class. On the contrary, the recall represents the ratio of the true positive cases (tp) according to the set of true-positive

Received: Added at production | Revised: Added at production | Accepted: Added at production
DOI: xxx/xxxx

and false-negative cases. The F-measure is expressed as:

$$\text{F1 score} = (1+\beta^2) \times \frac{\text{precision} \times \text{recall}}{(\beta^2 + \text{precision}) + \text{recall}} \quad (13)$$

where precision and recall are defined as:

$$\text{precision} = \frac{\text{TPR}}{\text{TPR+FPR}}, \quad (14)$$

$$\text{recall} = \frac{\text{TPR}}{\text{TPR+FNR}} \quad (15)$$

F-measure is considered a significant measure since it combines recall and precision values into a single effectiveness parameter. In the present work, the parameter of β is set to 1.

When applied to the testing samples, the performance measures of all conducted algorithms are presented in Table III. Table III indicates that ensemble learning models (RF and AdaBoost) achieved satisfactory detection results. The RF algorithm reached an AUC of 0.980 and the AdaBoost an AUC of 0.986. This could be attributed to their use of several weak learners (Trees in this case), which reduces the classification error. From Table III, one can observe the highest performance assessments of 0.993 and AUC of 0.993. Accordingly, the GAN-based approach offers a robust recognition of samples touched by desertification with few false-negative cases (i.e., FPR=0.011) and large detection ratio (i.e., TPR=0.997) even with challenging pixels presenting a high degree of similarity with desertified pixels, corresponding to like-desertification cases (like deforestation cases). One can also notice from Table VI that DBN, DBM, and CNN can achieve high identification rates by reaching an AUC of 0.980, 0.988, and 0.988, respectively. Generally speaking, the GAN remains considerably superior compared to the other considered classifiers (i.e., AUC=0.993). The GAN classification outperformed the other methods since GAN possesses an unconventional strategy in identifying desertification episodes. Notably, the GAN represents an efficient deep learning model that can learn complex data representations and capture data distributions without any need for labeling in an unsupervised manner, which makes its application suitable for solving complex classification problems such as separating desertified pixels from like-desertification samples. Furthermore, GAN learns to approximate the training dataset probability distribution by generating samples near the training dataset. Finally, the association GAN-Softmax allows the algorithm to act like a supervised algorithm, which learns how to classify the given input by providing a probability for each class.

TABLE 3 EVALUATION METRICS OF THE PROPOSED APPROACH COMPARED TO DBN, DBM, CNN, RF AND ADABOOST.

Model	TPR	FPR	Accuracy	Precision	F1Score	AUC
DBN	0.976	0.015	0.9805	0.984	0.98	0.9805
DBM	0.999	0.023	0.988	0.8	0.988	0.988
CNN	0.994	0.018	0.988	0.98	0.98	0.988
RF	0.973	0.014	0.980	0.986	0.979	0.980
AdaBoost	0.979	0.007	0.986	0.993	0.986	0.986
GAN	**0.997**	**0.011**	**0.993**	**0.989**	**0.993**	0.993

Figure 6 represents a visual progression of sand evolution during the whole studied period. Regions affected by desertification are presented with yellow dots. As a first remark, one can perceive the propagation of sand where numerous areas were invaded during the whole studied

Received: Added at production | Revised: Added at production | Accepted: Added at production
DOI: xxx/xxxx

interval of time (2000-2019). These affected areas principally represent one of these thematic classes: bare soil, less dense vegetation, or even rocky. Also, it can be noticed that the focal period of sand invasion happened between the years 2000 and 2006. The cause for this fast propagation of sand can be associated with diverse natural and human factors. For human factors, there is (i) unordered urban growth and (ii) incorrect exploitation of semi-vegetal and vegetal areas. While, natural factors are essentially associated to (i) wind direction, which favors the movement of sand and its invasion, in addition to (ii) the local topographic aspect characterized by the sloping terrain and (iii) the location of Mountains of Aurés in the north direction makes them play the role of windbreaks, which favors the sand accumulation in the area.

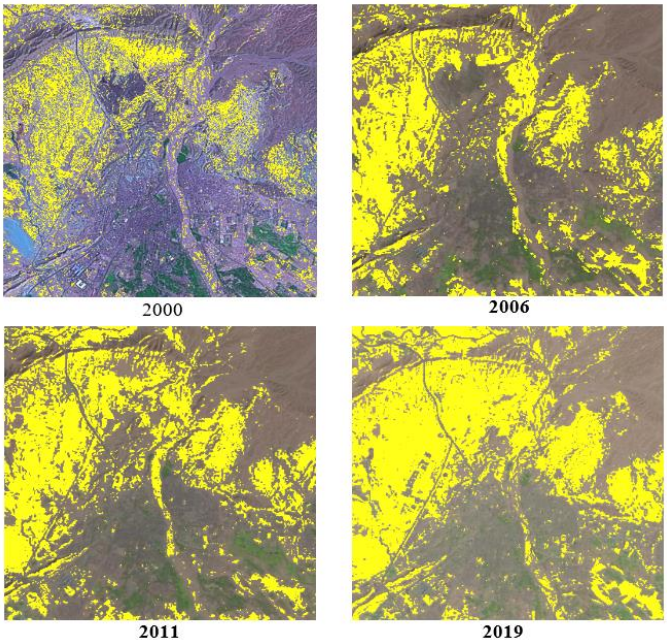

Figure 6 The Progression of Pixels Changed by Desertification During the Period (2000-2019).

Table IV compares the proposed classification strategy with some powerful state-of-the-art approaches using different classifiers, namely decision-tree [1], SVM [8], CNN [14], decision tree and Isodata combination [16]. For each work, the extracted features, the applied approach, the used dataset, and the obtained OA are reported.

Table 4 Evaluation metrics of the proposed approach compared to the state-of-the-art.

Classifier	The used features	Approach	Database	Accuracy (%)
Li et al., [1]	Spectral mixture analysis	Decision-tree	Landsat TM/ETM+ images	80
Afrasinei et. al[16]	Principal Components Analysis (PCA) & Knepper ratios	Decision tree & Isodata	Landsat 7 and 8 imagery	79.97
Ainiwaer et al. [14]	Typical plant species features and image backgrounds	CNN VGG 16	Optical UAV remote-sensing images	93.8
		CNN VGG 19		96.73
Azzouzi et. al [8]	Radiometric values	SVM	Optical satellite images (Landsat program)	95.15
The proposed method	**Multi-spectral and multi-temporal radiometric values**	**GAN**	**Optical satellite images (Landsat program)**	**99.3**

Received: Added at production | Revised: Added at production | Accepted: Added at production
DOI: xxx/xxxx

The reported results in Table IV indicate the outperformance of the GAN-based desertification approach compared to other investigated methods in detecting desertification cases. In the case of the decision-tree algorithm (applied alone [1] or combined with Isodata in [16], one can observe numerous misclassification cases, which affects the accuracy presenting a relatively low value (accuracy around 80%). In the study presented in [14], where deep learning approach using the CNN algorithm has been applied, the recognition level is comparatively acceptable, with an OA of 96.73% is obtained (with VGG 19). However, this separation is applied on sub-images instead of pixels as samples, making the segmentation stage indispensable to define the different sub-images. On the other hand, it is well-known that the segmentation phase applied in various topics is confusion-prone (where segmentation errors can directly affect the recognition rates).

In the proposed study in [8], desertified pixels were detected via an object-based approach by applying SVMs as a classification methodology. The obtained results in this study showed certain efficiency in the separation of desertified pixels, where accuracy of 95.15% is obtained. This efficiency is because of the consideration of the geometric distribution factor in the separation phase and opting for a sparse resolution by using structural risk minimization.

Finally, from Table IV, one can deduce that the GAN formalism outperformed the rest of compared studies by achieving a satisfying recognition rate of 99.3%. This outperformance makes GAN more adapted to discriminate desertified pixels from unchanged cases and provides a promising way to desertification detection application than other classification methods.

4 | CONCLUSION

Accurate desertification detection is undoubtedly an essential indicator to cope with desertification propagation. This paper caters to an effective data-driven deep learning approach that leverages the Landsat imagery and GAN-based deep learning paradigm for desertification detection. It is worth noting that the adversarial training way of both the generator and the discriminator in the GAN model could mine process nonlinearity and high cross-correlation in multivariate data and surpass the overfitting problem. The Softmax function uses the output layer of the GAN model to uncover desertification propagation. The GAN-based procedure is applied to multitemporal and multispectral remote sensing data to detect and discriminate land cover changes due to the sand propagation process in Biskra (Algeria) for 19 years (from 2000–2019). The results reveal that in comparison to other advanced deep learning algorithms, including DBM, DBN, and CNN, as well as two ensemble machine learning models (i.e., RF and AdaBoost), the GAN-based model has superior detection performance. Results demonstrate that the proposed GAN-based approach can separate desertification events from other land cover changes like deforestation or areas undergoing seasonal phenomena of wild grasses' dryness.

To enhance desertification detection, as a perspective of this work, we intend to incorporate several sensitive parameters for sand region characterization, namely NDVI, TGSI, LST, Albedo, and MSAVI.

DATA AVAILABILITY STATEMENT

The multi-temporal satellite images dataset that supports the findings of this study has been extracted from a publicly available archive of the United States Geological Survey (USGS) (https://earthexplorer.usgs.gov/). Several search criteria are combined to obtain remote sensing scenes covering the same study area of Biskra.

Received: Added at production | Revised: Added at production | Accepted: Added at production
DOI: xxx/xxxx

REFERENCES

[1] Li, J., Zhao, L., Xu, B., Yang, X., Jin, Y., Gao, T., & Qin, Z, 2014. Spatiotemporal variations in grassland desertification based on landsat images and spectral mixture analysis in Yanchi County of Ningxia, China. IEEE Journal of Selected Topics in Applied Earth Observations and Remote Sensing, 7(11), 4393-4402.

[2] Martínez-Valderrama, J., Ibáñez, J., Del Barrio, G., Sanjuán, M.E., Alcalá, F.J., Martínez-Vicente, S., Ruiz, A. and Puigdefábregas, J., 2016. Present and future of desertification in Spain: Implementation of a surveillance system to prevent land degradation. Science of the Total Environment, 563, pp.169-178.

[3] Jiang, L., Bao, A., Jiapaer, G., Guo, H., Zheng, G., Gafforov, K., Kurban, A. and De Maeyer, P., 2019. Monitoring land sensitivity to desertification in Central Asia: Convergence or divergence?. Science of the Total Environment, 658, pp.669-683.

[4] Harrou, F., Zerrouki, N., Sun, Y., & Hocini, L., 2018. Monitoring land-cover changes by combining a detection step with a classification step. IEEE Symposium Series on Computational Intelligence (SSCI). 1651-1655.

[5] Salvati, L., Mavrakis, A., Colantoni, A., Mancino, G. and Ferrara, A., 2015. Complex Adaptive Systems, soil degradation and land sensitivity to desertification: A multivariate assessment of Italian agro-forest landscape. Science of the Total Environment, 521, pp.235-245.

[6] Zerrouki, N., Harrou, F., & Sun, Y., 2018. Statistical monitoring of changes to land cover. IEEE Geoscience and Remote Sensing Letters, 15(6), 927-931.

[7] Zerrouki, N., Harrou, F., Sun, Y., & Hocini, L., 2019. A Machine Learning-Based Approach for Land Cover Change Detection Using Remote Sensing and Radiometric Measurements. IEEE Sensors Journal, 19(14), 5843-5850.

[8] Azzouzi, S. A., Vidal-Pantaleoni, A., & Bentounes, H. A., 2017. Desertification monitoring in Biskra, Algeria, with Landsat imagery by means of supervised classification and change detection methods. IEEE Access, 5, 9065-9072.

[9] Wang, Y. and Bai, L., 2019. Fuzzy Spatiotemporal Data Modeling Based on UML. IEEE Access, vol. 7, pp. 45405-45416, , doi: 10.1109/ACCESS.2019.2908224.

[10] Guan, Y., He, B., Li, X., Yin, C., & Qiu, S., 2017. Desertification assessment and trend analysis using modis data. IEEE International Geoscience and Remote Sensing Symposium (IGARSS) (pp. 5739-5742). IEEE.

[11] Lamchin, M., Lee, J. Y., Lee, W. K., Lee, E. J., Kim, M., Lim, C. H., & Kim, S. R., 2016. Assessment of land cover change and desertification using remote sensing technology in a local region of Mongolia. Advances in Space Research, 57(1), 64-77.

[12] Kundu, A., Patel, N. R., Saha, S. K., & Dutta, D., 2017. Desertification in western Rajasthan (India): an assessment using remote sensing derived rain-use efficiency and residual trend methods. Natural Hazards, 86(1), 297-313.

[13] Zanchetta, A., Bitelli, G., & Karnieli, A., 2016. Monitoring desertification by remote sensing using the Tasselled Cap transform for long-term change detection. Natural Hazards, 83(1), 223-237.

[14] Ainiwaer, M., Ding, J., & Kasim, N., 2020. Deep learning-based rapid recognition of oasis-desert ecotone plant communities using UAV lowaltitude remote-sensing data. Environmental Earth Sciences, 79, 1-11.

Received: Added at production | Revised: Added at production | Accepted: Added at production
DOI: xxx/xxxx

[15] Guo, B., & Wen, Y., 2019. An optimal monitoring model of desertification in Naiman Banner based on feature space utilizing Landsat8 OLI image. IEEE Access, 8, 4761-4768.

[16] Afrasinei, G. M., 2016. Study of land degradation and desertification dynamics in North Africa areas using remote sensing techniques.

[17] N. Boulghobra, T. Hadri, and M. Bouhana, 2014. Using Landsat imagery for monitoring the spatiotemporal evolution of sanding in dry land, the case of in-Salah in the Tidikelt (Southern Algerian Sahara). Geograph. Techn., vol. 9, no. 1,. 1-9.

[18] Nag, S., Hewagama, T., Georgiev, G. T., Pasquale, B., Aslam, S., & Gatebe, C. K., 2017. Multispectral snapshot imagers onboard small satellite formations for multi-angular remote sensing. IEEE Sensors Journal, 17(16), 5252-5268.

[19] Zerrouki, N., & Bouchaffra, D., 2014. Pixel-based or Object-based: Which approach is more appropriate for remote sensing image classification?. IEEE International Conference on Systems, Man, and Cybernetics (SMC). 864-869.

[20] T. Tieleman and G. Hinton, 2012. Lecture 6.5-rmsprop: Divide the gradient by a running average of its recent magnitude," COURSERA: Neural networks for machine learning, vol. 4, no. 2, 26–31.

[21] Zerrouki, Y., Harrou, F., Zerrouki, N., Dairi, A., & Sun, Y., 2020. Desertification Detection using an Improved Variational AutoEncoder-Based Approach through ETM-Landsat Satellite Data. IEEE Journal of Selected Topics in Applied Earth Observations and Remote Sensing.

[22] Zeroual, A., Harrou, F., Dairi, A. and Sun, Y., 2020. Deep learning methods for forecasting COVID-19 time-Series data: A Comparative study. Chaos, Solitons & Fractals, 140, p.110121.

[23] Harrou, F., Sun, Y., Hering, A.S. and Madakyaru, M., 2020. Statistical process monitoring using advanced data-driven and deep learning approaches: theory and practical applications. Elsevier.

[24] Dairi, A., Harrou, F., Sun, Y. and Khadraoui, S., 2020. Short-term forecasting of photovoltaic solar power production using variational auto-encoder driven deep learning approach. Applied Sciences, 10(23), p.8400.

[25] Goodfellow, I.J., Pouget-Abadie, J., Mirza, M., Xu, B., Warde-Farley, D., Ozair, S., Courville, A. and Bengio, Y., 2014. Generative adversarial networks. arXiv preprint arXiv:1406.2661.

[26] Zhang, Z., Xie, Y. and Yang, L., 2018. Photographic text-to-image synthesis with a hierarchically-nested adversarial network. In Proceedings of the IEEE Conference on Computer Vision and Pattern Recognition (pp. 6199-6208).

[27] Di, X., Zhang, H. and Patel, V.M., 2018, October. Polarimetric thermal to visible face verification via attribute preserved synthesis. In 2018 IEEE 9th International Conference on Biometrics Theory, Applications and Systems (BTAS) (pp. 1-10). IEEE.

[28] Ledig, C., Theis, L., Huszár, F., Caballero, J., Cunningham, A., Acosta, A., Aitken, A., Tejani, A., Totz, J., Wang, Z. and Shi, W., 2017. Photo-realistic single image super-resolution using a generative adversarial network. In Proceedings of the IEEE conference on computer vision and pattern recognition (pp. 4681-4690).

Received: Added at production | Revised: Added at production | Accepted: Added at production
DOI: xxx/xxxx

[29] Harrou, F., Dairi, A., Sun, Y. and Kadri, F., 2018. Detecting abnormal ozone measurements with a deep learning-based strategy. IEEE Sensors Journal, 18(17), pp.7222-7232.

[30] Dairi, A., Cheng, T., Harrou, F., Sun, Y. and Leiknes, T., 2019. Deep learning approach for sustainable WWTP operation: A case study on data-driven influent conditions monitoring. Sustainable Cities and Society, 50, p.101670.

[31] Dairi, A., Harrou, F., Senouci, M. and Sun, Y., 2018. Unsupervised obstacle detection in driving environments using deep-learning-based stereovision. Robotics and Autonomous Systems, 100, pp.287-301.

[32] Purwins, H., Li, B., Virtanen, T., Schlüter, J., Chang, S.Y. and Sainath, T., 2019. Deep learning for audio signal processing. IEEE Journal of Selected Topics in Signal Processing, 13(2), pp.206-219.

[33] Chen, S., Ren, H., Tao, Y., Zheng, Y., Sun, Y., Nie, J., ... & Fan, W., 2019,. A New Index for Sandy Land Detection Based On Thermal Infrared Emissivity Data. IEEE International Geoscience and Remote Sensing Symposium, IGARSS, 1402-1405.

[34] Ding, C., Liao, M., Zhang, L., Dong, J., & Feng, G., 2019. Quantifying Dynamic Characteristics of Dune Migration in Northwestern China with Multitemporal Optical Satellite Observations. IEEE International Workshop on the Analysis of Multi temporal Remote Sensing Images (MultiTemp) (pp. 1-4).

[35] Creswell, A., White, T., Dumoulin, V., Arulkumaran, K., Sengupta, B. and Bharath, A.A., 2018. Generative adversarial networks: An overview. IEEE Signal Processing Magazine, 35(1), pp.53-65.

[36] Zhu, L., Chen, Y., Ghamisi, P. and Benediktsson, J.A., 2018. Generative adversarial networks for hyperspectral image classification. IEEE Transactions on Geoscience and Remote Sensing, 56(9), pp.5046-5063.